

Tristability between Spots, Stripes, and Gaps

D. Wetzel

Institut für Mathematik, Universität Oldenburg, 26111 Oldenburg, Germany.

(Dated: 14th December 2024)

Third order amplitude equations on hexagonal lattices can be used for predicting the existence and stability of stripes, gaps, and spots in pattern forming systems. These amplitude equations predict the nonexistence of bistable ranges between gaps and spots and tristable ranges between stripes, gaps, and spots. In contrast, numerical studies show the existence of such tristable ranges. In the present work we use amplitude equations up to the fifth order for finding such bistable and tristable ranges. Furthermore, we use numerical path following methods to check the correctness of these analytical predictions.

INTRODUCTION

It was shown by Turing [1] in 1952 that nonhomogeneous steady states arise in reaction-diffusion systems when a homogeneous state is unstable for the full system and stable for the kinetics. This discovery was followed by a large number of works, where systems of different scientific disciplines such as biology [2, 3], chemistry [4–7], ecology [8–10], and physics [11, 12] are studied for so-called Turing patterns.

Typical 2D Turing patterns are stripes, gaps, and spots, which are also referred to as labyrinth patterns, down-, and up-hexagons, respectively. Stability transitions for such patterns are studied via expanding amplitude equations up to the third order in [13]. These amplitude equations predict that spots and gaps corresponding to the same wavenumber cannot be stable at the same time. In contrast, a tristable range between stripes, gaps, and spots for a specific system modeling vegetations of semiarid ecosystems is found in [9] via using numerical time integration.

The main result of the present work is that tristable ranges between stripes, gaps, and spots can be predicted by using amplitude equations up to the fifth order. The present work is organized as follows. We start with a quick review of amplitude equation reductions up to the third order. After this we show a bifurcation diagram for which we used numerical continuation methods for following the stripe, gap, and spot branches bifurcating from a homogeneous state of the vegetation model mentioned above and observe a tristable range as well. In order to predict tristable ranges we use a generalized Swift-Hohenberg equation for which we are able to reduce the full equation to a system of amplitude equations up to the fifth order. In the following a comparison of these predictions with numerical solutions is performed which shows that these amplitude equations give acceptable predictions.

AMPLITUDE EQUATIONS UP TO THE THIRD ORDER

Consider

$$u_t = D\Delta u + f(u, \lambda), \quad (1)$$

where u is a function $u : \mathbb{R}^2 \times \mathbb{R}_{>0} \rightarrow \mathbb{R}^n$, $\lambda \in \mathbb{R}$ a control parameter, $D \in \mathbb{R}^{n \times n}$, $\Delta = \partial_x^2 + \partial_y^2$, and t the time. Let u^* be a homogeneous state of (1) and (u_c^*, λ_c) a Turing point with corresponding critical wavenumber k_c . Finding approximations of patterned solutions near λ_c of the form

$$u = u^* + (A_1 e_1 + A_2 e_2 + A_3 e_3) \Phi + \text{c.c.} + \text{h.o.t.} \quad (2)$$

with $u^*, \Phi \in \mathbb{C}^n$, $e_j = e^{i(x,y) \cdot \mathbf{k}_j}$, $A_j = A_j(t) \in \mathbb{C}$ for $j = 1, 2, 3$,

$$\mathbf{k}_1 = k_c \begin{pmatrix} 1 \\ 0 \end{pmatrix}, \quad \mathbf{k}_2 = \frac{k_c}{2} \begin{pmatrix} -1 \\ \sqrt{3} \end{pmatrix}, \quad \text{and} \quad \mathbf{k}_3 = \frac{k_c}{2} \begin{pmatrix} -1 \\ -\sqrt{3} \end{pmatrix}$$

via reducing the full system to a system of amplitude equations given by

$$\begin{aligned} \dot{A}_1 &= c_1 A_1 + c_2 \overline{A_2 A_3} + c_3 A_1 |A_1|^2 \\ &\quad + c_4 A_1 (|A_2|^2 + |A_3|^2), \\ \dot{A}_2 &= c_1 A_2 + c_2 \overline{A_1 A_3} + c_3 A_2 |A_2|^2 \\ &\quad + c_4 A_2 (|A_1|^2 + |A_3|^2), \\ \dot{A}_3 &= c_1 A_3 + c_2 \overline{A_1 A_2} + c_3 A_3 |A_3|^2 \\ &\quad + c_4 A_3 (|A_1|^2 + |A_2|^2), \end{aligned} \quad (3)$$

is described in [12, 14]. Typical time independent solutions of (3) are up-hexagons H^+ , stripes S , and down-hexagons H^- for which the triple (A_1, A_2, A_3) is given by (h^+, h^+, h^+) , $(s, 0, 0)$, (h^-, h^-, h^-) , respectively. Here $h^+ \in \mathbb{R}_{>0}$, $s \in \mathbb{R}$, and $h^- \in \mathbb{R}_{<0}$. Their stability can be obtained from the Jacobian of (3). Unfortunately the amplitude reduction is only valid for small amplitudes (near λ_c), and if the quadratic terms of (2) are small.

Stability transitions between H^+ , S , and H^- via varying c_1 and c_2 are discussed in [13] and the following result is pointed out. For fixed parameters c_1, c_2, c_3, c_4, c_5 for which the three states H^+ , S , and H^- exist, the system (3) can only predict one of the following situations:

- only one of the states H^+ , S , H^- is stable (monostable case),
- S and H^+ or H^- are stable (bistable case),
- all three states are unstable.

Thus, bistable ranges between H^+ and H^- and tristable ranges between H^+ , S , and H^- are not predictable using (3).

The following vegetation model for semi-arid ecosystems

$$\begin{aligned} n_t &= \Delta n + \left(\frac{\gamma\omega}{1 + \sigma\omega} - \nu \right) n - n^2, \\ w_t &= \delta\Delta(\omega - \beta n) + p - (1 - \rho n)w - w^2 n \end{aligned} \quad (4)$$

is discussed in [9] and used in [13] to apply the amplitude reduction and compare it with numerical results. Here n , w , and p represent the vegetation density, ground water density, and precipitation, respectively. p is used as a control parameter. The other parameters are given by

$$\gamma = \sigma = 1.6, \nu = 0.2, \rho = 1.5, \beta = 3, \delta = 100. \quad (5)$$

Please see [9] for modeling details and the meaning of these parameters. Numerical time integration methods are used in [9] to follow the stable parts of stripes and up- and down-hexagons by varying p in both directions and to see where transitions between these patterns occur. Here, a tristable range between H^+ , S , and H^- is observed. In the present work we use numerical path following methods to calculate the corresponding branches and observe a tristable range as well (see Fig.1).

We also see in Fig.1 that the stripes bifurcate subcritically, turn around in a fold, and become stable after this fold. Since the amplitude equations (3) are only expanded up to third order terms, the fold and consequently the stable stripes cannot be described via (3). The parameter δ is changed for the applications in [13] such that both Turing points come closer together and stripes bifurcate supercritically, which makes the amplitude reduction valid for the whole existence regions of H^+ , S , and H^- .

AMPLITUDE EQUATIONS UP TO THE FIFTH ORDER

We have seen above that the amplitude equation reduction up to the third order on a hexagonal lattice does not predict the tristability of H^+ , S , and H^- , but a tristable range for the reaction-diffusion system (4) is found numerically on bounded domains. In the present section we show that tristable ranges can be predicted via amplitude equations up to the fifth order. Such an expansion is only valid for special systems and unfortunately

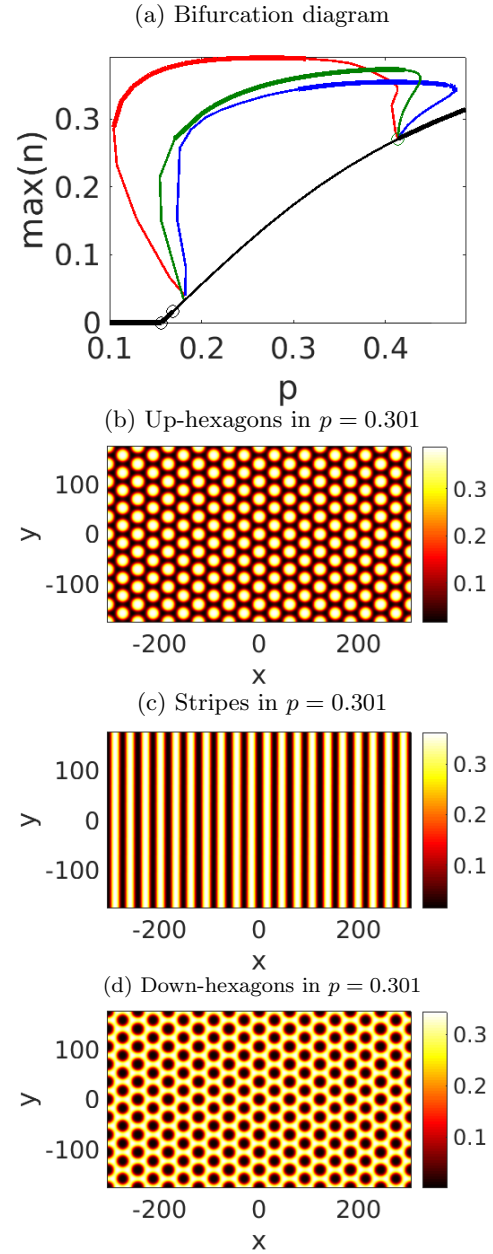


Figure 1. The system (4) for the parameter set (5) has one trivial homogeneous state $(n, w) = (0, p)$, which is stable for small p and becomes unstable for large p . At this transition of stability a nontrivial homogeneous state bifurcates, which is stable at the beginning, becomes Turing unstable a bit later and becomes stable again later on. The black lines in (a) represent both homogeneous states. Here and in the following thick and thin lines represent stable and unstable states, respectively. We use the continuation and bifurcation software tool pde2path [15, 16] to follow the solution branches which bifurcate in the second Turing point. Here we use the domain $\Omega = (-l_x, l_x) \times (-l_y, l_y)$ with $l_x = 20\pi/k_c$, $l_y = 20\pi/(\sqrt{3}k_c)$ and Neumann boundary conditions, while $k_c = 0.206$ is the critical wavenumber corresponding to the second Turing point. The red, green, and blue branches in (a) correspond to H^+ , S , and H^- , respectively. Here we can see that there is a small tristable range. All three states are stable for $p = 0.301$ and their density plots for n are shown in (b)-(d).

not for (4) so that we consider the following generalized Swift-Hohenberg equation

$$u_t = [\varepsilon^4 c_1 - (1 + \Delta)^2]u + \varepsilon^3 c_2 u^2 + \varepsilon^2 c_3 u^3 + \varepsilon c_4 u^4 + c_5 u^5 \quad (6)$$

with $c_1, c_2, c_3, c_4, c_5 \in \mathbb{R}$ and $\varepsilon \in \mathbb{R}_{>0}$.

(6) has the trivial solution $u = 0$ which has a Turing bifurcation in $c_1 = 0$. Furthermore, (6) is scaled with ε such that an amplitude equation reduction up to the fifth order is possible and valid for small ε . To do so we use the ansatz (2) with $\Phi = \varepsilon$ and $u^* = 0$ and end up with the following amplitude equation system

$$\begin{aligned} \dot{A}_1 &= c_1 A_1 + 2c_2 \overline{A_2 A_3} + 3c_3 A_1 |A_1|^2 \\ &\quad + 6c_3 A_1 (|A_2|^2 + |A_3|^2) + D_1, \\ \dot{A}_2 &= c_1 A_2 + 2c_2 \overline{A_1 A_3} + 3c_3 A_2 |A_2|^2 \\ &\quad + 6c_3 A_2 (|A_1|^2 + |A_3|^2) + D_2, \\ \dot{A}_3 &= c_1 A_3 + 2c_2 \overline{A_1 A_2} + 3c_3 A_3 |A_3|^2 \\ &\quad + 6c_3 A_3 (|A_1|^2 + |A_2|^2) + D_3 \end{aligned} \quad (7)$$

with $D_i = 12 c_4 C_{4i} + c_5 C_{5i}$ for $i = 1, 2, 3$,

$$\begin{aligned} C_{41} &= A_1^2 A_2 A_3 + (2|A_1|^2 + |A_2|^2 + |A_3|^2) \overline{A_2 A_3}, \\ C_{42} &= A_2^2 A_1 A_3 + (|A_1|^2 + 2|A_2|^2 + |A_3|^2) \overline{A_1 A_3}, \\ C_{43} &= A_3^2 A_1 A_2 + (|A_1|^2 + |A_2|^2 + 2|A_3|^2) \overline{A_1 A_2}, \end{aligned}$$

and

$$\begin{aligned} C_{51} &= 30 \overline{A_1} \overline{A_2} \overline{A_3}^2 + 10 A_1 (|A_1|^4 + 3|A_2|^4 + 3|A_3|^4 \\ &\quad + 6|A_1|^2 |A_2|^2 + 6|A_1|^2 |A_3|^2 + 12|A_2|^2 |A_3|^2), \\ C_{52} &= 30 \overline{A_2} \overline{A_1} \overline{A_3}^2 + 10 A_2 (3|A_1|^4 + |A_2|^4 + 3|A_3|^4 \\ &\quad + 6|A_1|^2 |A_2|^2 + 12|A_1|^2 |A_3|^2 + 6|A_2|^2 |A_3|^2), \\ C_{53} &= 30 \overline{A_3} \overline{A_1} \overline{A_2}^2 + 10 A_3 (3|A_1|^4 + 3|A_2|^4 + |A_3|^4 \\ &\quad + 12|A_1|^2 |A_2|^2 + 6|A_1|^2 |A_3|^2 + 6|A_2|^2 |A_3|^2). \end{aligned}$$

To see if H^+ , S , and H^- are stable or not in their existence range, we split the amplitudes in (7) into real and imaginary parts and gain a system with 6 equations and thus a state of (7) has 6 eigenvalues. We fix c_3 , c_4 , c_5 and determine regions of stability depending on c_1 and c_2 (see Fig.2(a)). Besides monostable and bistable ranges between stripes and hexagons, we found tristable ranges and bistable ranges between H^+ and H^- . We also fix c_2 and use pde2path for comparing analytical and numerical solutions, while c_1 is used as a control parameter (see Fig.2(b)). Here we see that (7) gives reasonable predictions.

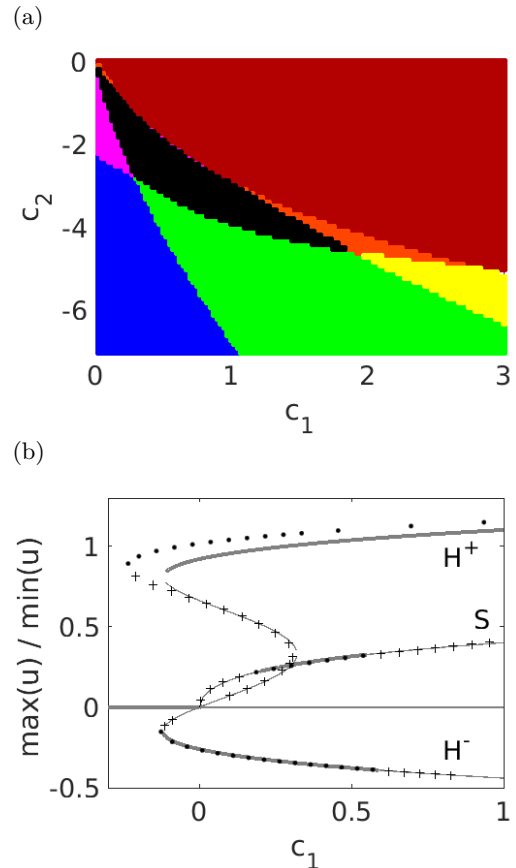


Figure 2. We set $c_3 = -1$, $c_4 = 5$, $c_5 = -2$ for creating the plots in the present figure. We vary c_1 and c_2 and determine H^+ , S , and H^- and their stability via (7) for creating (a). H^+ , S , and H^- are monostable in the red, yellow, and blue regions, respectively. We have bistable ranges between H^- and S , H^- and H^+ , H^+ and S in the green, violet, and orange regions, respectively. In the black regions all three states are stable. We set $c_2 = -2$ for creating (b) and use c_1 as a control parameter. Here we use the amplitude equations (7) for creating the solid lines. \bullet and $+$ represent stable and unstable states, respectively, which we found numerically via the finite element and Newton's method on the domain $\Omega = (-l_x, l_x) \times (-l_y, l_y)$ with $l_x = 10\pi$, $l_y = 10\pi/\sqrt{3}$ and Neumann boundary conditions. Here we use $\varepsilon = 0.5$. The vertical axis shows the maximum of u for stripes and up-hexagons and the minimum of u for down-hexagons.

- [1] A. M. Turing, Philosophical transaction of the Royal Society of London - B **237**, 37 (1952).
- [2] A. Gierer and H. Meinhardt, *Kybernetik*, Biological Cybernetics **12**, 30 (1972).
- [3] J. Murray, *Mathematical biology* (Springer-Verlag, Berlin, 1989).
- [4] I. Berenstein, L. Yang, M. Dolnik, A. M. Zhabotinsky, and I. R. Epstein, *Physical review letters* **91**, 058302 (2003).
- [5] L. Yang, M. Dolnik, A. M. Zhabotinsky, and I. R. Ep-

stein, Chaos: An Interdisciplinary Journal of Nonlinear Science **16**, 037114 (2006).

[6] M. Leda, V. K. Vanag, and I. R. Epstein, Physical Review E **80**, 066204 (2009).

[7] T. Bánsági, V. K. Vanag, and I. R. Epstein, Science **331**, 1309 (2011).

[8] J. von Hardenberg, E. Meron, M. Shachak, and Y. Zarmi, Phys. Rev. Lett. **87**, 198101 (2001).

[9] E. Meron, E. Gilad, J. von Hardenberg, M. Shachak, and Y. Zarmi, Chaos, Solitons, and Fractals **19**, 367 (2004), fractals in Geophysics.

[10] H. Yizhaq, E. Gilad, and E. Meron, Physica A: Statistical Mechanics and its Applications **356**, 139 (2005).

[11] J. Swift and P. C. Hohenberg, Physical Review A **15**, 319 (1977).

[12] M. Golubitsky, J. W. Swift, and E. Knobloch, Physica D: Nonlinear Phenomena **10**, 249 (1984).

[13] K. Gowda, H. Riecke, and M. Silber, Phys. Rev. E **89**, 022701 (2014).

[14] R. Hoyle, *Pattern formation* (Cambridge University Press., Cambridge, UK, 2006).

[15] H. Uecker, “www.staff.uni-oldenburg.de/hannes.uecker/pde2path/,” (2017).

[16] H. Uecker, D. Wetzel, and J. Rademacher, NMTMA **7**, 58 (2014).